Supporting information

Interfacial engineered Mo_2C/MoO_2 Heterojunction Electrocatalyst for Efficient Hydrogen Evolution in Alkaline Brine

Jiarong Mu, Xiaotong Xu, Jianfang Jing* and Yiguo Su*

Experimental section

1.1. Chemicals

All chemicals were analytically pure without further purification. Milli-Q ultra-pure water (18.25 MΩ·cm) was used for all experimental procedures. Ethanol [(C_2H_5OH), ≥99.7%], hydrochloric acid [(HCl), 37%] nickel ammonium molybdate [($(NH_4)_6Mo_7O_{24}·4H_2O$), 99%] and dopamine hydrochloride were obtained from Tianjin Fengchuan Chemical Reagent Co. Ltd., China. Ammonia water [$NH_3·H_2O$, 28%] Nickel foam (NF) were purchased from Beijing Innochem Technology Co., Ltd. Potassium hydroxide [(KOH), 99.99%], Pt/C were obtained from Alfa Aesar.

1.2. Materials characterization details

X-ray diffraction (XRD) was conducted using a PuXi XD3 diffractometer that was equipped with Cu Ka radiation and featured a graphite monochromator. (k = 0.15406 nm). The overall morphology, as well as the particle size distribution and selected area electron diffraction analysis of the material, were performed using a transmission electron microscope. The instrument utilised for this study was a FEI Tecnai G2 F20 S-TWIN, with an acceleration voltage of 200 kV and a point resolution of 0.24 nm. Prior

to testing, powder samples were subjected to ultrasonic dispersion in ethanol, dispensed onto ultrathin carbon-coated copper grids, dried, and mounted on sample holders. Morphology and structure were primarily observed using bright-field imaging mode. In order to facilitate the resolution of the lattice structure of materials at the atomic scale and to observe interplanar spacings, lattice defects (such as dislocations and twins) and interface structures, high-resolution transmission electron microscopy (HR-TEM) analysis was performed. All measurements were conducted on the same instrument (FEI Tecnai G2 F20 S-TWIN, 200 kV). HR-TEM imaging demands a sample thickness and stability that is extremely high, necessitating the selection of uniform and sufficiently thin regions (typically near the edges). By precisely adjusting the objective current to the Scherzer defocus condition, lattice fringe patterns were obtained. The captured images evidently demonstrate the arrangement of atomic crystal planes. The identification of specific crystal planes is achieved through the measurement of lattice fringe spacings, which are then compared with those documented in standard PDF cards. In order to obtain atomic number contrast images of nanomaterials and perform elemental distribution analysis, a high-angle annular dark-field scanning transmission electron microscopy (HAADF-STEM) mode was employed. The present study was conducted on the aforementioned TEM platform (FEI Tecnai G2 F20 S-TWIN) at an operating voltage of 200 kV. The HAADF detector collects electrons scattered at high angles (typically >50 mrad), with its imaging intensity approximating proportionality to the square of atomic number (Z^2). This provides excellent compositional contrast, making it particularly suitable for observing

interfaces in metal-loaded nanoparticles, heterostructures, or composite materials. During the testing process, samples are typically dispersed onto an ultrathin carbon-coated copper mesh. In probe correction mode, a focused electron beam performs a two-dimensional scan of the sample while simultaneously acquiring HAADF signals, yielding Z-contrast images with sub-nanometer resolution. When this is combined with an energy-dispersive spectrometer (EDS) for area scanning, it is possible to perform further qualitative and semi-quantitative mapping of elemental composition distribution. The X-ray photoelectron spectroscopy (XPS) analysis was conducted using Thermo ESCALAB 250 to examine the surface electronic states and chemical composition of the samples.

1.3. Electrochemical test details

Electrochemical experiments of all three-electrode systems were performed on the CHI760E electrochemical workstation. The working electrode contained each of the catalysts synthesized, and the reference and counter electrodes were Hg/HgO electrode and carbon rod, respectively. All observed potentials vs. Hg/HgO were calibrated to a reversible hydrogen electrode (RHE) according to ERHE = $E_{Hg/HgO}$ + 0.059 × pH + 0.098. Firstly, the catalysts were electrochemically activated via cyclic voltammetry (CV) at a scan rate of 50 mV s^{-1} until the electrodes reached a steady state. During the linear scanning voltametric (LSV) curves tests, we used a scan rate of 5 mV s^{-1} with 95% IR-compensation. The Tafel slope was estimated by means of the Tafel equation: $\eta = a \times \log j + b$, where η, j, a, and b represent the overpotential, current density, constant, and Tafel slope, respectively. The CV curves at different scan rates

were tested in the non-Faraday region to estimate the double-layer capacitance (C_{dl}). Electrochemical impedance spectroscopy (EIS) tests were performed at 5 mV^{-1} amplitude, 0.01 Hz to 100 kHz frequency. To further evaluate the stability, long duration chronopotentiometry tests were performed at constant current densities of 1000 mA cm^{-2}.

TOF calculation. The TOF is calculated by followed Equation S1-S4:

$$\text{TOF} = \frac{\text{NH}_{2\text{ per unit area}}}{\text{N}_{\text{active site per unit area}}} \quad \text{Equation}$$

$$\text{NH}_{2\text{ per unit area}} = \left(|J|\frac{\text{mA}}{\text{cm}^{-2}}\right)\left(\frac{1\text{Cs}^{-1}}{1000\text{ mA}}\right)\left(\frac{1\text{ mol e}^{-1}}{96485.3\text{ C}}\right)\left(\frac{1\text{ mol}}{2\text{ mol e}^{-1}}\right)\left(\frac{6.022\times10^{23}\text{mo}}{1\text{ mol}}\right.$$

$$= 3.12\times10^{15}\frac{\text{S}^{-1}}{\text{cm}^2}|J| \quad \text{Equation S2}$$

$$\text{N}_{\text{active site per unit area}} = \text{N}_{\text{Mo atom}}$$

$$= \left(\frac{\text{catalyst loading per unit area}\left(\text{x g cm}^{-2}\right)\times\text{Pt wt.\%}}{\text{Mo M}_\text{w}\left(\text{g mol}^{-1}\right)}\right)\left(\frac{6.022\times10^{23}\text{Mo atoms}}{1\text{ mol Mo}}\right)$$

Equation S3

Where J is the measured current density. M_w is the atomic mass of Mo.

For example, the $N_{\text{active site per unit area}}$ for Mo_2C/MoO_2@NC was calculated from:

$$N_{\text{active site per unit area}} = \left(\frac{2.78 \times 10^{-3}\,\text{g cm}^{-2} \times 44\ \text{wt.\%}}{95.95\ \text{g mol}^{-1}}\right)\left(\frac{6.022 \times 10^{23}\ \text{Mo atoms}}{1\ \text{mol Mo}}\right) = 7.67 \times 10^{18}\ \text{cm}^{-2}$$

Hence, the TOF for Mo_2C/MoO_2@NC can be calculated from:

$$\text{TOF} = \frac{3.12 \times 10^{15}\ \frac{\text{s}^{-1}}{\text{cm}^2}}{7.67 \times 10^{18}\ \text{cm}^{-2}} \times |J| = 0.000407 \times |J|\,\text{s}^{-1} \quad \text{(Equ. S4)}$$

2.1. Sample preparation

2.1.1. Pretreatment of nickel foam (NF)

The 3 × 4 cm NF were sonicated in 3 M HCl for 30 min and then washed with ultrapure water. Subsequently, the NF were sonicated in three solutions of acetone, ethanol, and ultrapure water for 30 min. Finally, the NF were dried under vacuum conditions at 60 °C for 3 h.

2.1.2. Pretreatment of Mo-PDA

Weigh 120 mg of ammonium molybdate and dissolve it in 32 mL of deionized water (referred to as Solution A). Weigh 120 mg of dopamine hydrochloride and dissolve it in 64 mL of anhydrous ethanol (referred to as Solution B). The two solutions were vigorously stirred for 30 min each, forming uniform, colorless, transparent solutions. Then slowly add Solution B to Solution A, causing the solution to turn orange and turbid. Add 0.6 mL of 28 wt% ammonia solution to the mixture, stir for 6 hours,

and centrifuge to obtain an orange precipitate. Finally, wash the precipitate three times with deionized water and anhydrous ethanol, respectively, dry overnight at 60 °C, yielding Mo-PDA.

2.1.3 Pretreatment of Mo_2C/MoO_2@NC

The obtained Mo-PDA was subjected to high-temperature calcination under argon atmosphere protection at 900 °C for 2 h with a heating rate of 5 °C /min, yielding Mo_2C/MoO_2@NC.

2.1.4 Pretreatment of Mo_2C

Initially, a solution comprising 1.2 g of ammonium molybdate and 0.3 g of glucose is to be prepared by dissolving the components in 25 mL of deionized water. It is imperative that the substance is sonicated for a duration of 30 minutes in order to ensure complete dissolution and dispersion. The mixture should subsequently be transferred to a 50 mL hydrothermal reactor, where it should be left to react at 180 °C for a period of 12 hours. Subsequent to the reaction, the product must be collected by centrifugation and dried over the course of an overnight period at a temperature of 60°C. The final step in the process is the calcination of the dried precursor in an argon atmosphere at a temperature of 900°C for a duration of two hours. This process is undertaken in order to obtain the Mo_2C material.

2.1.4 Pretreatment of MoO_2

Firstly, ammonium molybdate was subjected to heat treatment in a muffle furnace under an air atmosphere. The temperature was increased at a rate of 5 °C/min

until it reached 550 °C, after which the substance was left to cool. The result was white molybdenum trioxide (MoO_3) powder. Subsequently, the MoO_3 precursor was calcined at 550 °C for 3 hours under a reducing atmosphere (5% H_2/Ar mixture). This process ultimately yielded grey-black, metallic-luster molybdenum dioxide (MoO_2) powder.

2.1.5 Pretreatment of NC

The synthesis of nitrogen-doped carbon (NC) was achieved through the high-temperature pyrolysis of dopamine hydrochloride. The specific procedure is as follows: First, precisely weigh 120 mg of the dopamine hydrochloride precursor and place it in a quartz boat. Subsequently, under continuous argon gas flow protection, the sample was heated at a rate of 5 °C/min to 900 °C and held at this temperature for 2 h. After thermal treatment, the sample was allowed to cool naturally to room temperature within the furnace under an argon atmosphere. The resulting black solid powder constitutes the NC sample.

2.1.6. Preparation of the working electrode

Electrode preparation was undertaken using the standard drop-coating method. The specific steps are outlined below: Initially, 5 mg of catalyst powder was dispersed in a mixed solvent consisting of 10 μL of Nafion solution (5 wt%) and 100 μL of anhydrous ethanol. The mixture was then exposed to ultrasonic treatment for a duration of 30 minutes, followed by continuous dispersion via magnetic stirring for a period of 24 hours, with the objective of achieving a uniform and stable catalyst

suspension. Subsequently, a specific volume (typically 5-20 μL) of the suspension was dispensed using a micropipette and uniformly drop-coated onto the surface of a pre-cleaned and dried foam nickel substrate (geometric area: 0.3 cm^2). Subsequent to each coating, the electrode was permitted to dry naturally at ambient temperature. Subsequent to the complete evaporation of the solvent, the working electrode was obtained.

2.1.7. Preparation of the Brine water + 1 M KOH

All electrochemical tests described in this paper were conducted in a multicomponent alkaline suspension electrolyte. The specific preparation method for this electrolyte is outlined below: Initially, 11.22 g of solid potassium hydroxide (KOH) should be dissolved in approximately 150 mL of pre-cooled deionized water. This solution should then be stirred until it is fully dissolved, at which point it should be allowed to cool to room temperature. Once this base alkaline solution has been obtained, it can be used in the following steps. Subsequently, 8.0 g of sodium chloride (NaCl) and 6.0 g of anhydrous calcium chloride ($CaCl_2$) should be added sequentially, with stirring to ensure dissolution. The subsequent step involves the addition of 10.0 g of magnesium chloride hexahydrate ($MgCl_2 \cdot 6H_2O$). This results in the rapid formation of a substantial quantity of white magnesium hydroxide precipitate within the solution. Finally, 1.0 g of calcium sulfate dihydrate ($CaSO_4 \cdot 2H_2O$) powder should be added. The mixture should then be transferred to a 200 mL volumetric flask, diluted to volume with deionized water, and vigorously shaken to form a homogeneous suspension. The electrolyte under scrutiny is, by nominal definition, a 1 M KOH

solution, containing supersaturated Ca^{2+} and Mg^{2+} ions in conjunction with elevated concentrations of Na^{+}, Cl^{-}, and SO_4^{2-} ions. In reality, the system is heterogeneous, comprising $Mg(OH)_2$, $Ca(OH)_2$, and undissolved $CaSO_4$ solids. Prior to the commencement of the testing procedure, the electrolyte was subjected to rigorous agitation to ensure the homogeneity of the sample.

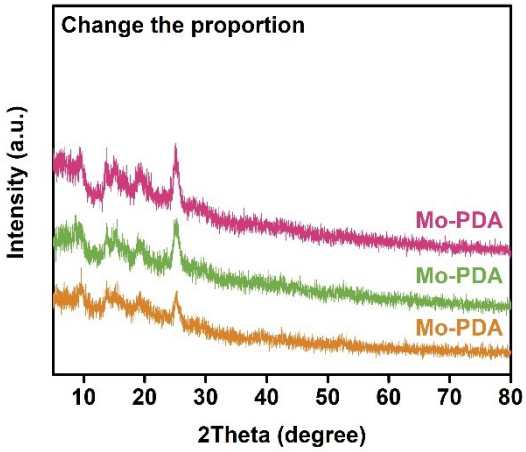

Fig. S1 XRD patterns of Mo-PDA.

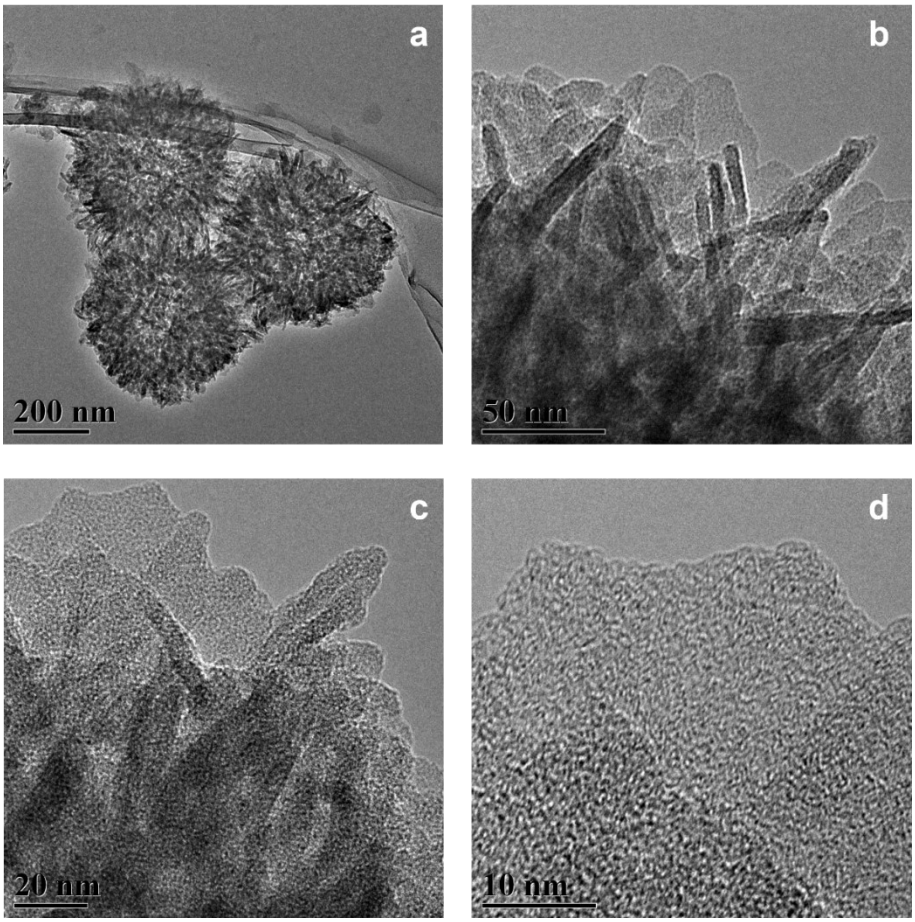

Fig. S2 TEM images of Mo-PDA.

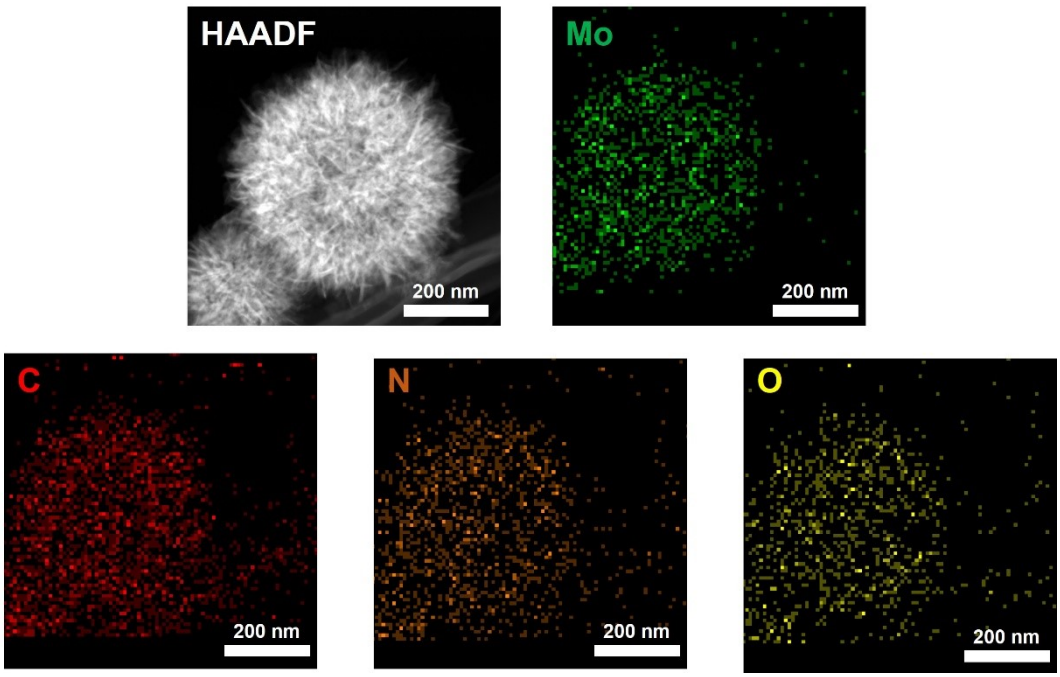

Fig.S3 HAADF-STEM images and corresponding elemental maps of Mo-PDA.

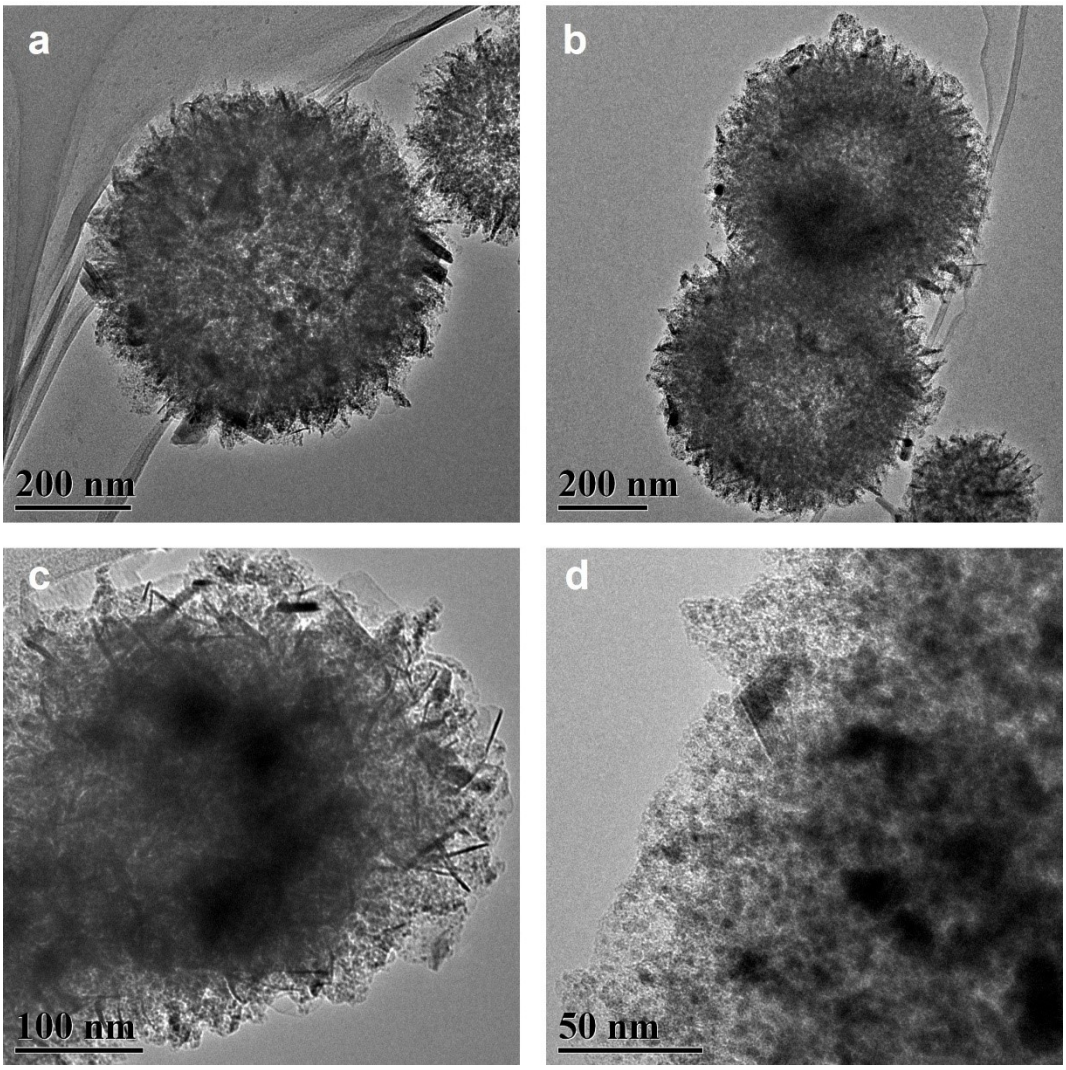

Fig. S4 TEM images of Mo_2C/MoO_2@NC.

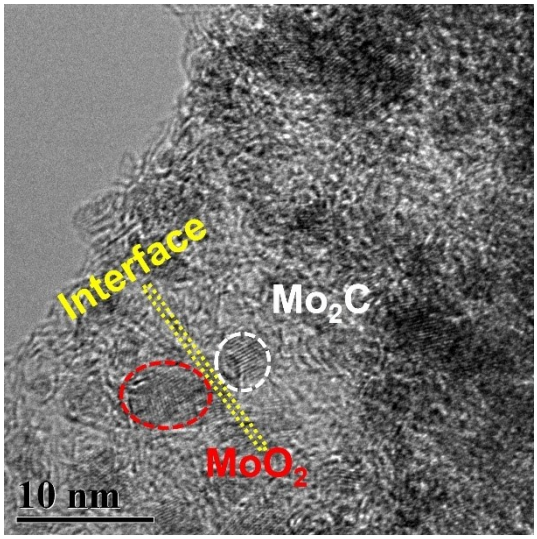

Fig. S5 HR-TEM image of Mo_2C/MoO_2@NC.

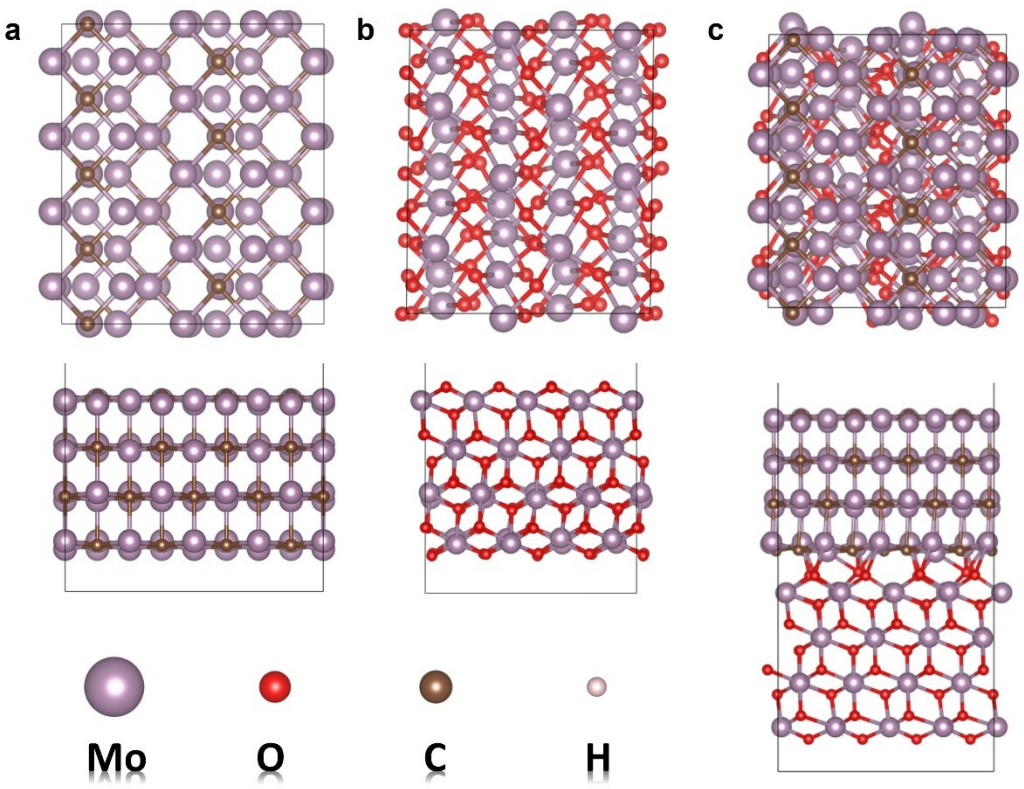

Fig. S6 The theoretical models of the optimized configurations of (a) Mo_2C, (b) MoO_2, (c) Mo_2C/MoO_2.

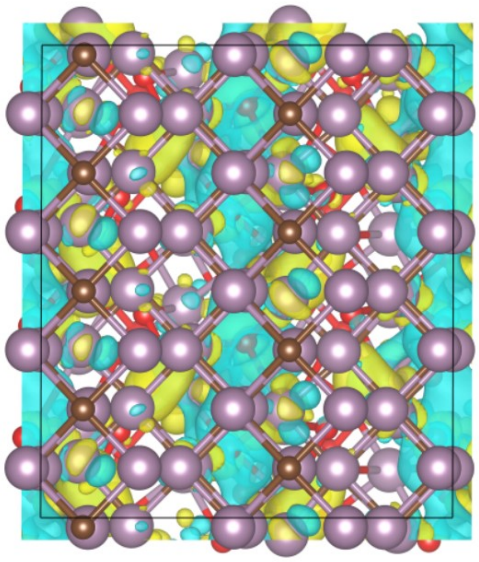

Fig. S7 Charge differential density of Mo_2C/MoO_2@NC.

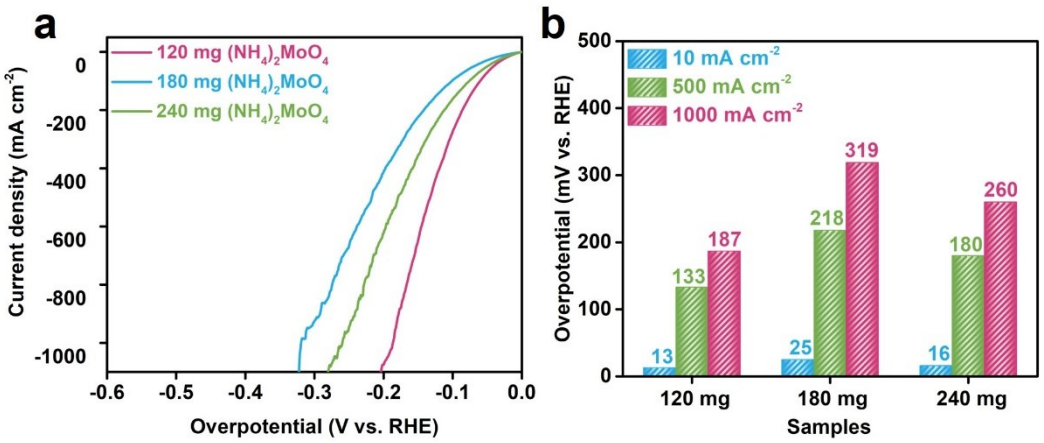

Fig. S8 (a) LSV curves, (b) overpotentials of catalysts with different proportions of ammonium molybdate in 1 M KOH.

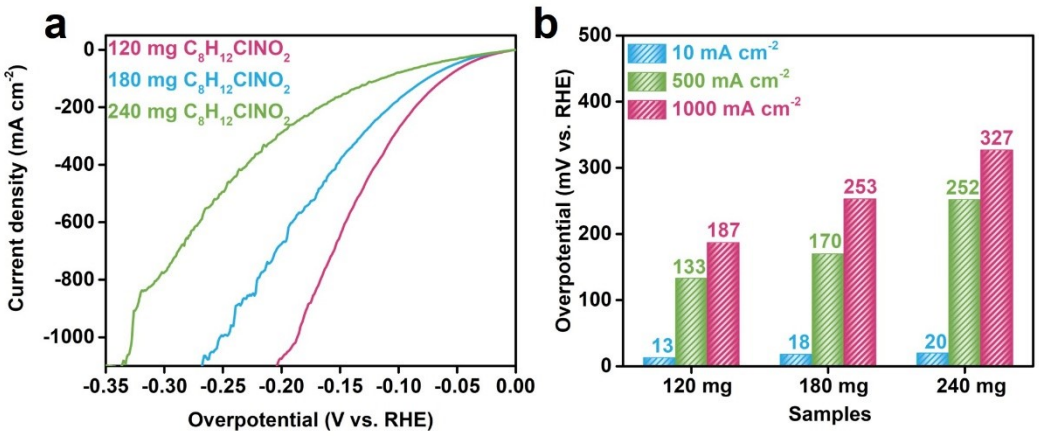

Fig. S9 (a) LSV curves, (b) overpotentials of catalysts with different proportions of dopamine hydrochloride in 1 M KOH.

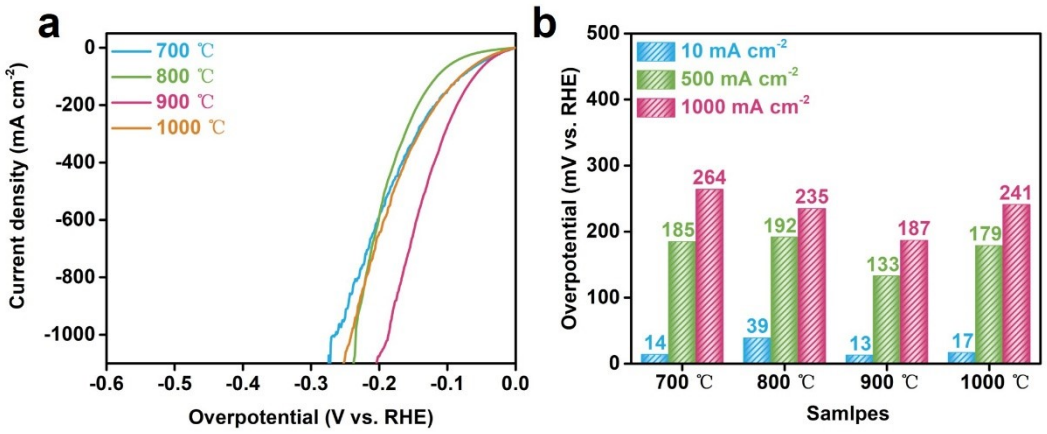

Fig. S10 (a) LSV curves, (b) overpotentials of catalysts with different sintering temperature in 1 M KOH.

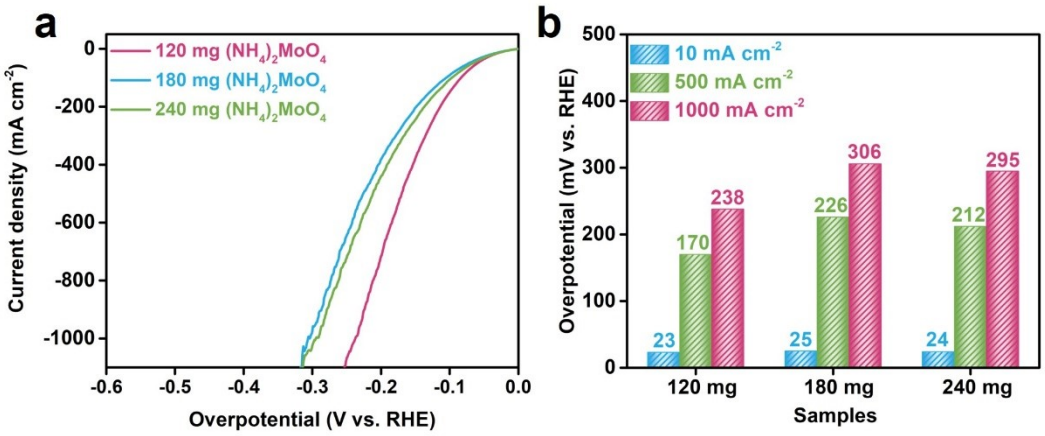

Fig. S11 (a) LSV curves, (b) overpotentials of catalysts with different proportions of ammonium molybdate in 1 M KOH + brine water.

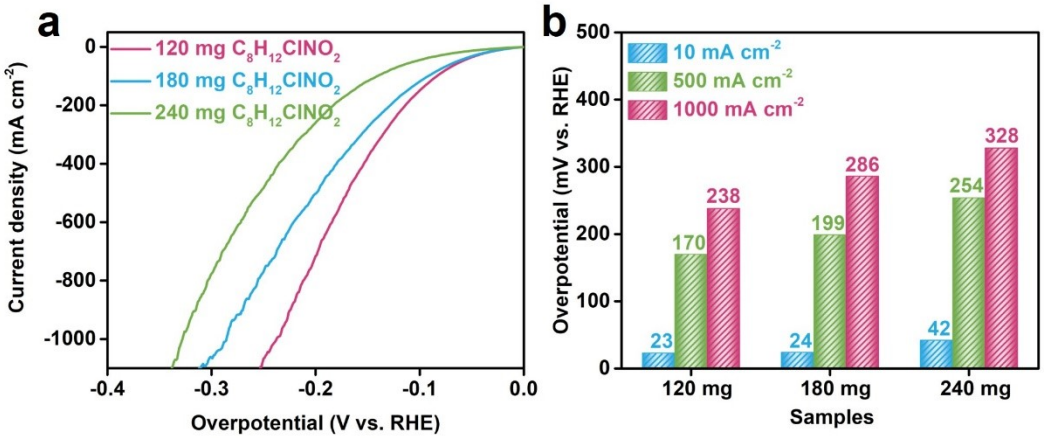

Fig. S12 (a) LSV curves, (b) overpotentials of catalysts with different proportions of dopamine hydrochloride in 1 M KOH + brine water.

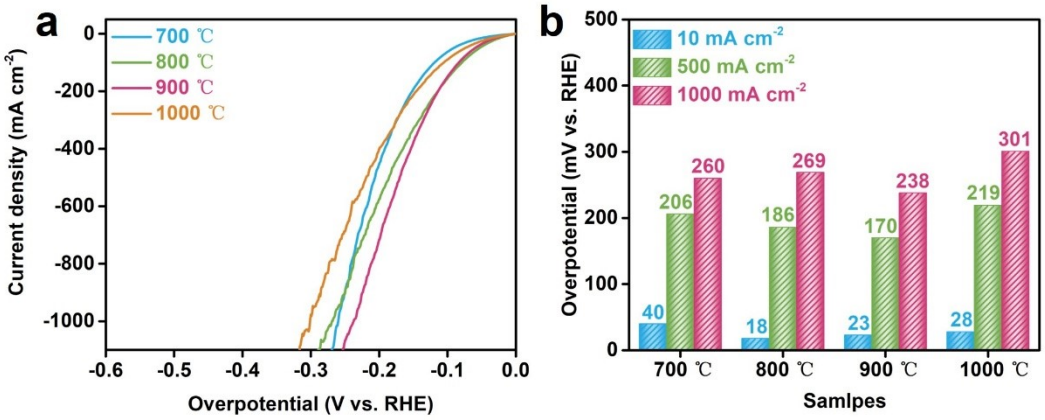

Fig. S13 (a) LSV curves, (b) overpotentials of catalysts with different sintering temperature in 1 M KOH + brine water.

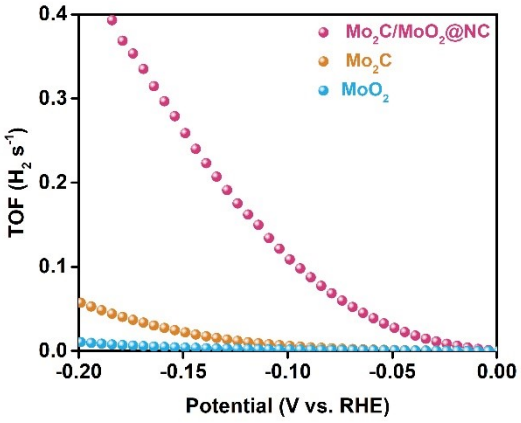

Fig. S14 TOF curve of Mo_2C/MoO_2@NC in 1 M KOH.

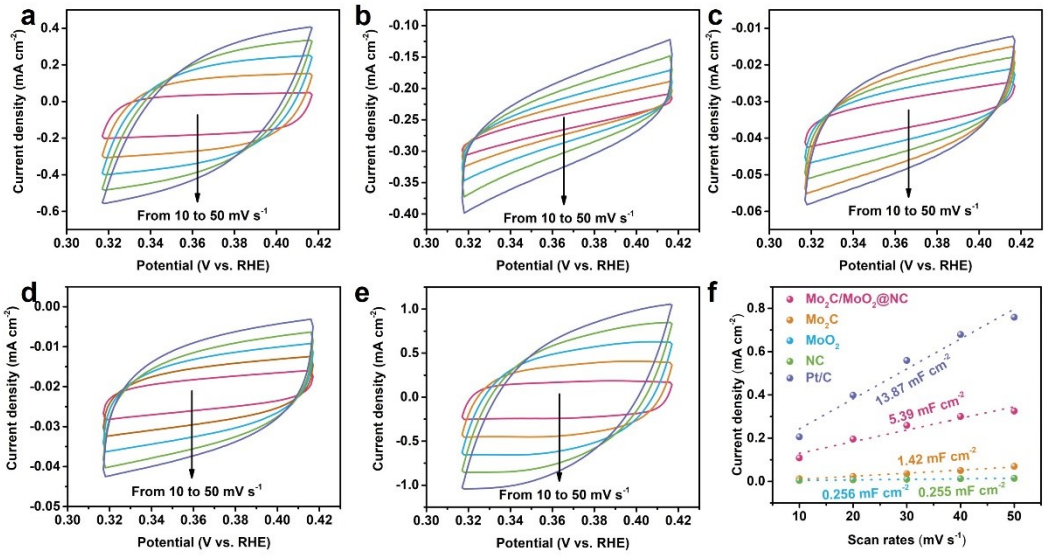

Fig. S15 CV curves for (a) Mo_2C/MoO_2@NC (b) Mo_2C, (c) MoO_2, (d) NC and (e) Pt/C catalysts at different scan rates from 10 to 50 mV s^{-1} in 1 M KOH, (f) The corresponded C_{dl} plots derived from CV curves.

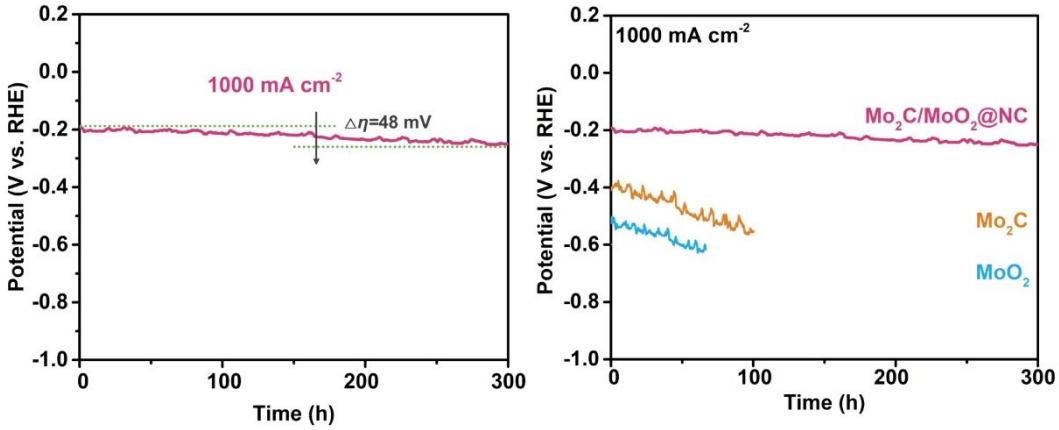

Fig. S16 Chronopotentiometry curves of Mo_2C/MoO_2@NC, Mo_2C, MoO_2 at 1000 mA cm^{-2} in 1 M KOH.

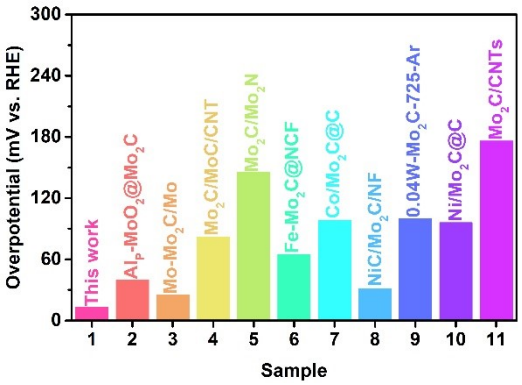

Fig. S17 Comparison of the overpotential at 10 mA cm^{-2} in 1 M KOH with the recently reported Mo-based catalysts.

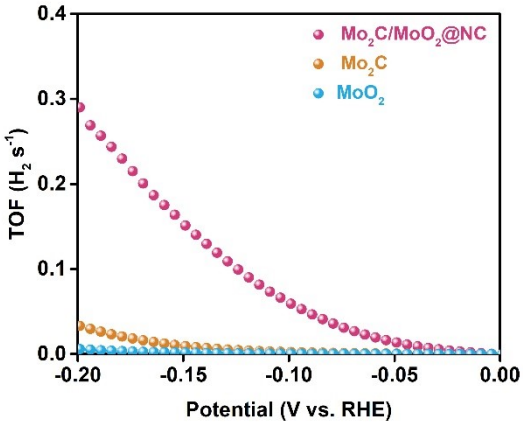

Fig. S18 TOF curve of Mo_2C/MoO_2@NC in 1 M KOH + brine water.

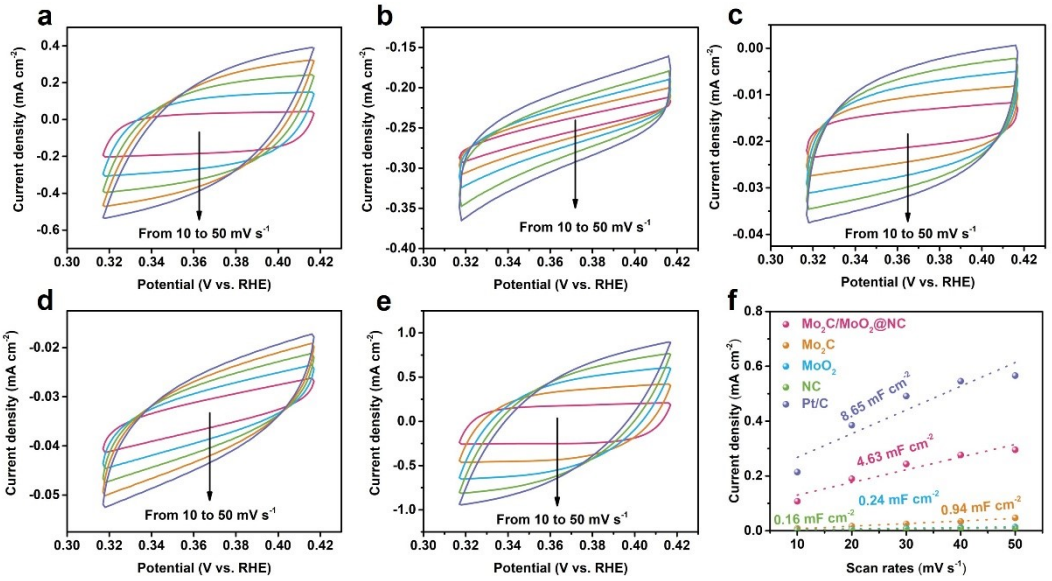

Fig. S19 CV curves for (a) Mo_2C/MoO_2@NC (b) Mo_2C, (c) MoO_2, (d) NC and (e) Pt/C catalysts at different scan rates from 10 to 50 mV s^{-1}. (f) The corresponded C_{dl} plots derived from CV curves in 1 M KOH + brine water.

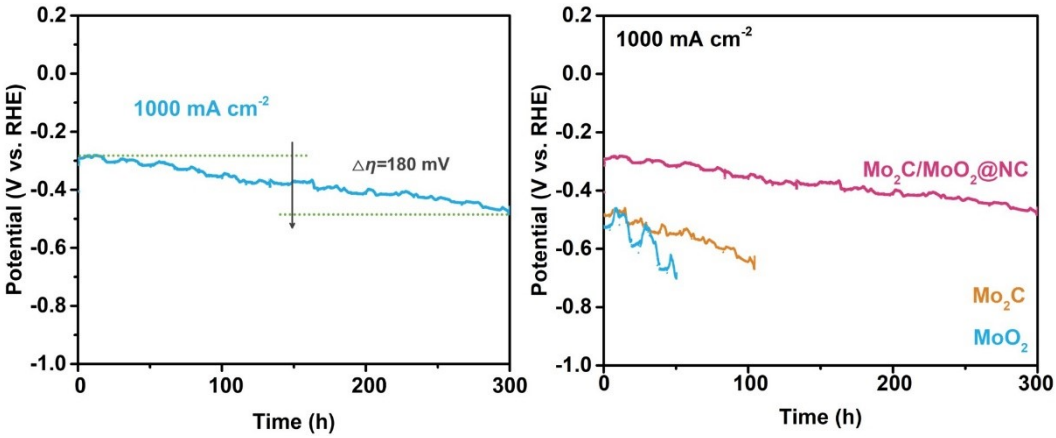

Fig. S20 Chronopotentiometry curves of Mo_2C/MoO_2@NC, Mo_2C, MoO_2 at 1000 mA cm^{-2} in 1 M KOH+ Brine water.

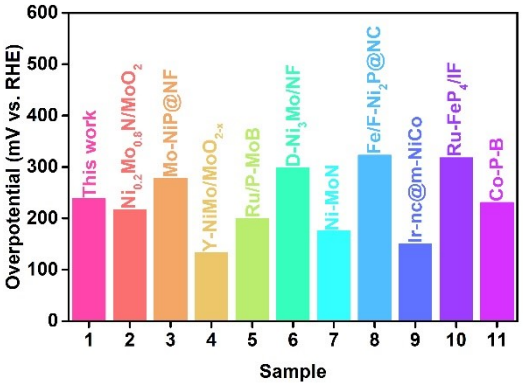

Fig. S21 Comparison of the overpotential at 1000 mA cm^{-2} in 1 M KOH + brine water with the recently reported catalysts.

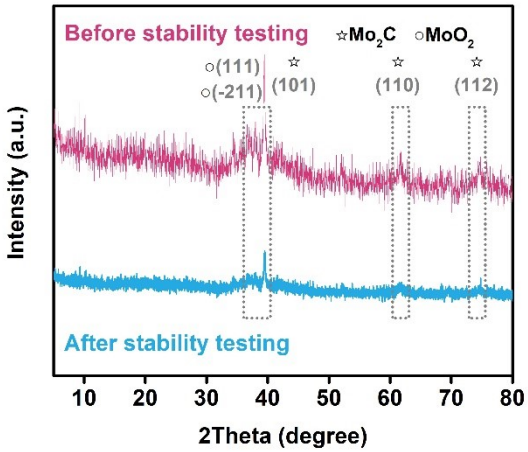

Fig. S22 XRD pattern of Mo_2C/MoO_2@NC before and after stability test.

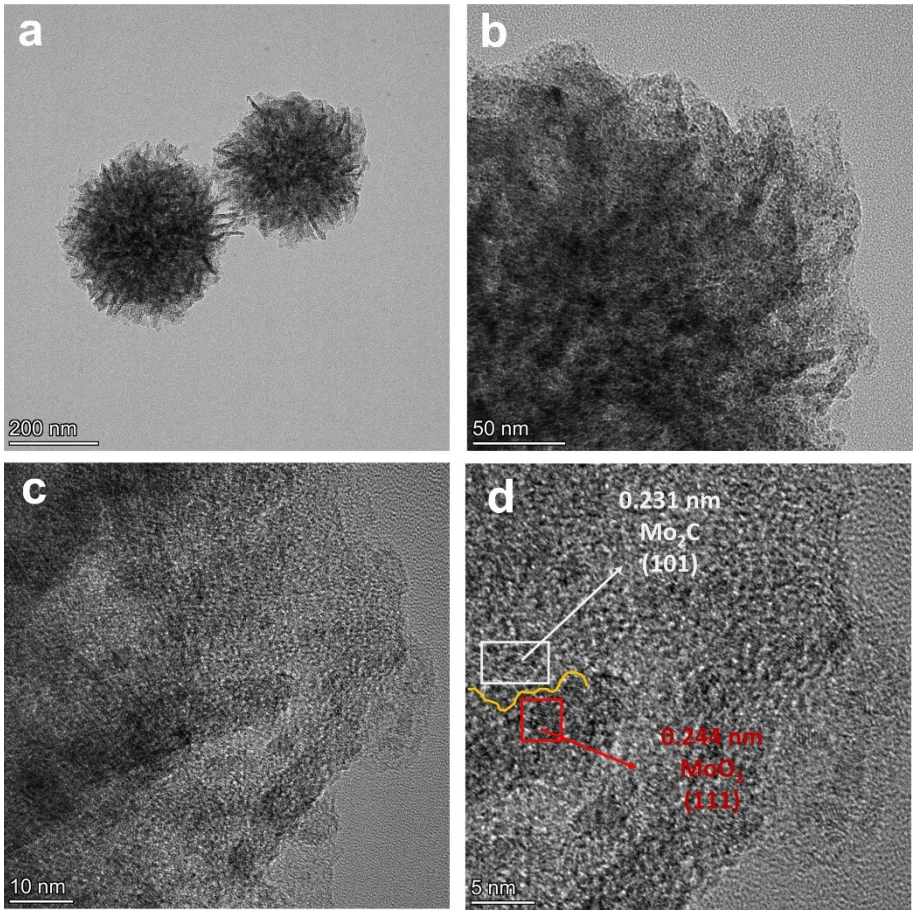

Fig. S23 TEM and HR-TEM images of Mo_2C/MoO_2@NC before and after stability test.

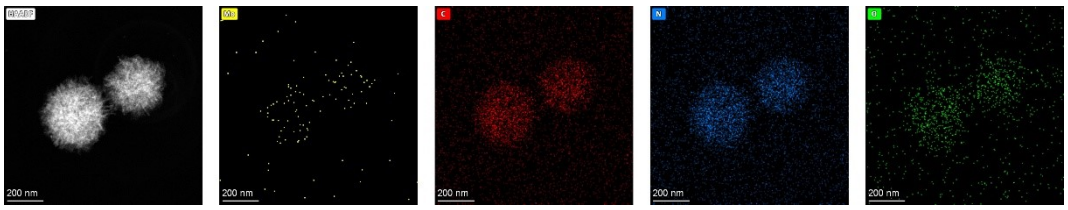

Fig. S24 HAADF-STEM images and corresponding elemental maps of Mo_2C/MoO_2@NC after stability test.

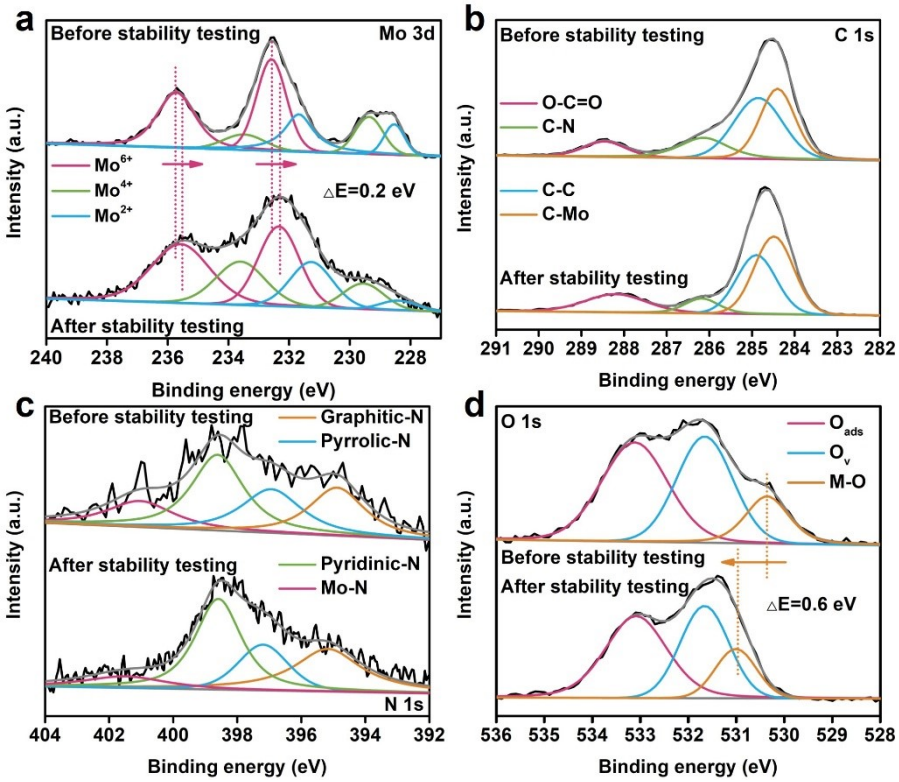

Fig. S25 XPS spectra of (a) Mo 3d, (b) C 1s, (c) N 1s and (d) O 1s for Mo_2C/MoO_2@NC before and after stability test.

Table S1. Comparison of catalytic performance of the Mo_2C/MoO_2@NC catalyst in 1 M KOH and the representative Mo_2C-based catalysts reported in the literatures.

Catalysts	Overpotential (mV@10 mA cm^{-2})	Tafel plots (mV/dec)	Stability (h)	References
Mo_2C/MoO_2@NC	13	49.75	300	This work
AlP-MoO_2@Mo_2C	40	40	200	1
Mo-Mo_2C/Mo	25	N.A.	360	2
Mo_2C/MoC/CNT	82	42	336	3
Mo_2C/Mo_2N	145	55	5.5	4
Fe-Mo_2C@NCF	65	41	12	5
Co/Mo_2C@C	98	68	48	6
NiC/Mo_2C/NF	31	63	200	7
0.04W-Mo_2C-725-Ar	99.86	60.16	20	8
Ni/Mo_2C@C	96	81	18	9
Mo_2C/CNTs	176	95	1	10

Table S2. Comparison of catalytic performance of the Mo_2C/MoO_2@NC catalyst in 1 M KOH + brine water and the representative Mo-based catalysts reported in the literatures.

Catalysts	Overpotential (mV@1 A cm^{-2})	Tafel plots (mV/dec)	Stability (h)	References
Mo_2C/MoO_2@NC	238	57.63	300	This work
$Ni_{0.2}Mo_{0.8}N/MoO_2$	217	146.8	200	11
Mo-NiP@NF	278	57.4	1500	12
Y-NiMo/MoO_{2-x}	133	22.7	2500	13
Ru/P-MoB	200	36	100	14
D-Ni_3Mo/NF	298	32.4	200	15
Ni-MoN	176	35.5	200	16
Fe/F-Ni_2P@NC	323	64.4	30	17
Ir-nc@m-NiCo	150	30.8	100	18
Ru-FeP_4/IF	318	51.58	20	19
Co-P-B	231	77	30	20

Reference

1. Z. Chen, M. Yang, Y. Li, W. Gong, J. Wang, T. Liu, C. Zhang, S. Hou, G. Yang, H. Li, Y. Jin, C. Zhang, Z. Tian, F. Meng, Y. Cui, *Nat. Commun.*, 2025, **16**, 418.
2. S. Yuan, L. Xiang, N. Li, T. Liang, K. Wang, X. Gao, M. Cui, L. Zhao, *Adv. Funct. Mater.*, 2025, **35**, 2422514.
3. C. Li, Z. Wang, M. Liu, E. Wang, B. Wang, L. Xu, K. Jiang, S. Fan, Y. Sun, J. Li, K. Liu, *Nat. Commun.*, 2022, **13**, 3338.
4. S. Li, C. Cheng, A. Sagaltchik, P. Pachfule, C. Zhao, A. Thomas, *Adv. Funct. Mater.*, 2019, **29**, 1807419.
5. J. Huang, J. Wang, R. Xie, Z. Tian, G. Chai, Y. Zhang, F. Lai, G. He, C. Liu, T. Liu, P. R. Shearing, D. J. L. Brett, *J. Mater. Chem. A*, 2020, **8**, 19879.
6. S. Yuan, M. Xia, Z. Liu, K. Wang, L. Xiang, G. Huang, J. Zhang, N. Li, *Chem. Eng. J.*, 2022, **430**, 132697.
7. S. Liu, N. Wang, G. Liu, S. Yang, C. Li, Y. Zhou, H. He, Y. Chen, K. Thummavichaia, Y. Zhu, *J. Colloid Interface Sci.*, 2024, **661**, 606-613.
8. W. Chen, M. Niu, Z. Zhang, L. Chen, X. Li, J. Zhang, R. Sun, H. Cao, X. Wang, *Small*, 2024, **20**, 2311026.
9. J. Wang, Y. Su, Y. Li, H. Li, J. Guo, Q. Sun, H. Hu, Y. Liu, X. Jia, Z. Jian, L. Kong, H. Liu, J. Li, H. Chu, S. Dou, Y. Xiao, *ACS Appl. Mater. Interfaces*, 2024, **16**, 2330−2340.
10. S. Majumdar, S. Chaitoglou, J. Serafin, G. Farid, R. Ospina, Y. Ma, R. A. Rovira, E. Bertran-Serra, *Int. J. Hyrog. Energy*, 2024, **89**, 977-989.
11. P. Lu, J. Huo, M. Cui, Y. Dou, W. Li, H. Liu, Z. Bai, S. Dou, R. Ge, *Adv. Funct. Mater.*, 2025, e16798.
12. W. Hao, X. Ma, L. Wang, Y. Guo, Q. Bi, J. Fan, H. Li, G. Li, *Adv. Energy Mater.*, 2025, **15**, 2403009.
13. S. Liu, Z. Zhang, K. Dastafkan, Y. Shen, C. Zhao, M. Wang, *Nat. Commun.*, 2025, **16**, 773.
14. P. Yang, F. Liu, X. Zang, L. Xin, W. Xiao, G. Xu, H. Li, Z. Li, T. Ma, J. Wang, Z. Wu, L. Wang, *Adv. Energy Mater.*, 2024, **14**, 2303384.
15. L. Xiao, T. Yang, C. Cheng, X. Du, Y. Zhao, Z. Liu, X. Zhao, J. Zhang, M. Zhou, C. Han, S. Liu, Y. Zhao, Y. Yang, H. Liu, C. Dong, J. Yang, *Chem. Eng. J.*, 2024, **485**, 150044.
16. L. Wu, F. Zhang, S. Song, M. Ning, Q. Zhu, J. Zhou, G. Gao, Z. Chen, Q. Zhou, X. Xing, T. Tong, Y. Yao, J. Bao, L. Yu, S. Chen, Z. Ren, *Adv. Mater.*, 2022, **34**, 2201774.
17. W. Zhang, X. Liu, Q. Yu, X. Wang, H. Mao, J. Chi, B. Li, J. Wan, L. Wang, *Chem. Eng. J.*, 2023, **454**, 140210.
18. J. Yuan, J. Zhou, Z. Peng, G. Li, Y. Hou, M. K. H. Leung, *J. Mater. Chem. A*, 2024, **12**, 2383.
19. T. Cui, J. Chi, J. Zhu, X. Sun, J. Lai, Z. Li, L. Wang, *Appl. Catal. B Environ. Energy*,

2022, **309**, 121950.

20. R. Silviya, A. Bhide, S. Gupta, R. Bhabal, K. H. Mali, B. R. Bhagat, M. Spreitzer, A. Dashora, N. Patel, R. Fernandes, *Small Methods*, 2024, **8**, 2301395.